INSTITUTE OF PHYSICS PUBLISHING NANOTECHNOLOGY
Nanotechnology **14** (2003) 1130–1139 PII: S0957-4484(03)61396-6

Raman spectroscopy for probing chemically/physically induced phenomena in carbon nanotubes

A G Souza Filho[1], A Jorio[2], Ge G Samsonidze[3], G Dresselhaus[4], R Saito[5] and M S Dresselhaus[3,6,7]

[1] Departamento de Física, Universidade Federal do Ceará, Caixa Postal 6030, 60455-900 Fortaleza, Ceará, Brazil
[2] Departamento de Física, Universidade Federal de Minas Gerais, 30123-970, Belo Horizonte, Brazil
[3] Department of Electrical Engineering and Computer Science, Massachusetts Institute of Technology, Cambridge, MA 02139-4307, USA
[4] Francis Bitter Magnet Laboratory, Massachusetts Institute of Technology, Cambridge, MA 02139-4307, USA
[5] Department of Physics, Tohoku University, and CREST, JST, Sendai 980-8578, Japan
[6] Department of Physics, Massachusetts Institute of Technology, Cambridge, MA 02139-4307, USA

E-mail: agsf@fisica.ufc.br, adojorio@fisica.ufmg.br, gsm@mgm.mit.edu, gene@mgm.mit.edu, saito@mgm.mit.edu and millie@mgm.mit.edu

Received 24 March 2003, in final form 7 July 2003
Published 5 September 2003
Online at stacks.iop.org/Nano/14/1130

Abstract
The use of recent advances in resonance Raman spectroscopy studies on isolated carbon nanotubes and the scientific knowledge achieved so far from these studies is discussed in the context of advancing carbon nanotube-based technology. Changes in the Raman spectra can be used to probe and monitor structural modifications of the nanotube sidewalls that come from the introduction of defects and the attachment of different chemical species. The former effect can be probed through the analysis of the disorder-induced Raman modes and the latter through the upshifts/downshifts observed in the various Raman modes due to charge transfer effects.

1. Introduction

Raman spectroscopy is nowadays well established as a powerful technique for characterizing a variety of carbon materials [1, 2], including their most famous nanostructured forms, namely fullerenes and carbon nanotubes (including both the single-wall and multiwall varieties in isolated or bundled forms) [3–5]. Carbon nanotubes are currently very important materials for the development of nanoscience and nanotechnology because of the new concepts that they have introduced, and because of the many technological applications envisioned for these materials owing to their unique physical properties. The Raman spectra for carbon nanotubes are unique, distinctive and significantly different from those of other forms of carbon due to the reduced dimensionality of carbon nanotubes. The Raman technique has been of particular importance because it allows one to get a rich, detailed characterization (structural, vibrational and electronic) of carbon nanotubes, perhaps more than with any other available characterization technique. This paper focuses on the scientific knowledge achieved so far by carrying out Raman spectroscopy studies on single-wall carbon nanotubes and how this knowledge might impact carbon nanotube-based technology. We will illustrate this focus by discussing the sensitivity of the Raman spectra to modifications of the nanotube surface, such as by the introduction of surface species and the charge transfer effects resulting from the chemical functionalization of nanotubes.

We first introduce in section 2 a brief description of nanotube properties that are relevant for our present discussion. In section 3 we briefly describe single-nanotube spectroscopy,

[7] Author to whom correspondence should be addressed.

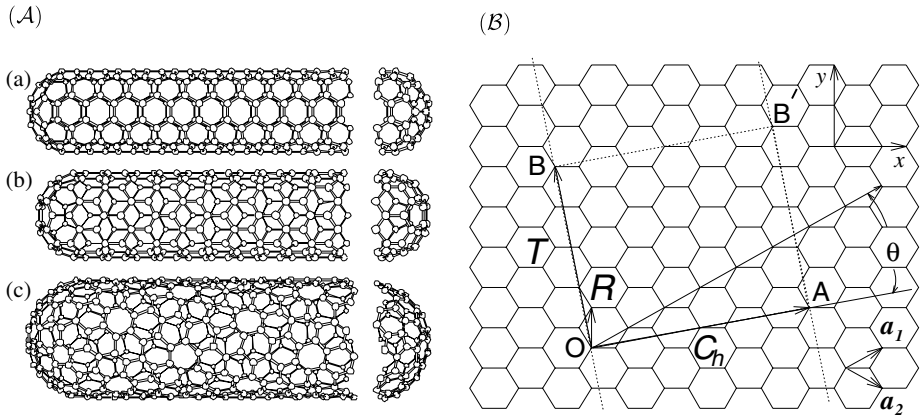

Figure 1. ($\mathcal{A}$) Classification of carbon nanotubes: (a) armchair, (b) zigzag and (c) chiral nanotubes. From the figure it can be seen that the orientation of the six-membered ring in the honeycomb lattice relative to the axis of the nanotube can be taken almost arbitrarily. ($\mathcal{B}$) The unrolled honeycomb lattice of a nanotube. When we connect sites O and A, and sites B and B', a seamless nanotube can be constructed. $\overrightarrow{OA}$ and $\overrightarrow{OB}$ define the chiral vector $\boldsymbol{C}_\mathrm{h}$ and the translation vector $\boldsymbol{T}$ of the nanotube, respectively. The rectangle $OAB'B$ defines the unit cell for the nanotube. The vector $\boldsymbol{R}$ denotes a symmetry vector that is used for generating the coordinates of carbon atoms in the nanotube.

that is the study of Raman spectra from one isolated nanotube. This *single-molecule spectroscopy* also provides a deeper understanding of bulk samples (nanotube ropes and bundles) that are already being used for several important technological applications. We also present the theoretical background on the disorder-induced modes. In section 4 we show how the features observed in the Raman spectra can be used to probe the effects of surface modifications, such as the introduction of defects and dopants, on the nanotube properties. Section 5 summarizes the main issues and points out some potential applications of Raman spectroscopy for carbon nanotube-based technology.

2. Structure and electronic properties of carbon nanotubes

A single-wall carbon nanotube can be considered to be a single atomic layer of 2D graphite (called a graphene sheet) rolled up into a seamless cylinder (figure 1($\mathcal{A}$)). The structure of each nanotube is uniquely described by two integers (n, m), which refer to the number of $\boldsymbol{a}_1$ and $\boldsymbol{a}_2$ unit vectors of the 2D graphene lattice that are contained in the chiral vector, $\boldsymbol{C}_\mathrm{h} = n\boldsymbol{a}_1 + m\boldsymbol{a}_2$, which spans the circumference of each nanotube (see figure 1($\mathcal{B}$)) [6]. These (n, m) indices also determine the nanotube diameter and chirality, or the orientation of the carbon hexagons with respect to the nanotube axis. The (n, m) indices carry information on all the structural, electronic and vibrational properties of the nanotube.

The electronic properties of SWNTs are remarkable insofar as they can be either metallic or semiconducting, depending on their (n, m) indices or chirality. Specifically, the SWNTs for which $(n - m) = 3p$ are metallic, while those for which $(n - m) = 3p \pm 1$ are semiconducting, where p is an integer. The energy bandgaps for semiconducting tubes typically are in the range of several hundreds of millielectron volts and exhibit a reciprocal diameter $1/d_\mathrm{t}$ dependence, thus allowing bandgap engineering to be carried out by selecting tubes with different diameters d_t. Furthermore, the electronic energy band structure and the density of electronic states are also uniquely determined by (n, m) [6]. The singularities in the density of states are called van Hove singularities (VHS) and they appear prominently as sharp peaks (typical of 1D systems) in the density of electronic states, as shown in figure 2(a) for three specific (n, m) single-wall metallic nanotubes. The semiconducting tubes also exhibit such a spiked density of states, but show a bandgap (no electronic states) between the first VHS singularity peaks in the valence and conduction band density of states, in contrast to metallic tubes which show a constant energy-independent density of states at the Fermi level E_F (see figure 2(a)). Typical magnitudes of this constant density of states is ∼0.03 states/carbon atom/eV for $d_\mathrm{t} \sim 1.4$ nm [7].

A very useful plot for analysing both Raman and optical measurements for bundled and isolated SWNT samples is the so-called Kataura plot [9], shown in figure 3, where the dependence of the electronic transitions labelled by E_{ii} from the ith valence band to the corresponding ith level in the conduction band for both semiconducting (superscript S) and metallic (superscript M) tubes is plotted as a function of the diameter d_t of the nanotube. The index i labels the flat region (maximum or minimum) of the nanotube subband dispersion relative to the Fermi level ($E = 0$), and the same index is used to designate both the valence and conduction subbands away from the Fermi level. The scatter of the points observed within each subband in figure 3 is due to the trigonal warping effect, or alternatively to the anisotropy, of the constant energy contours about the K point (the equi-energy contours develop a triangular shape when moving away from the K point), as depicted in figure 2(b). This anisotropy in the equi-energy contours is very special for Raman spectroscopy in the sense that each possible (n, m) pair has a unique set of energies E_{ii} where the VHS occur. This trigonal warping effect is very important for using Raman spectroscopy to perform a structural determination for individual nanotubes, because Raman spectra are observable only for those nanotubes that have E_{ii} energies close to the laser excitation energy E_laser. The case of isolated SWNTs provides detailed information about E_{ii} (through the resonant selectivity process) and d_t (through the frequency of the vibrational mode) simultaneously, thus providing all

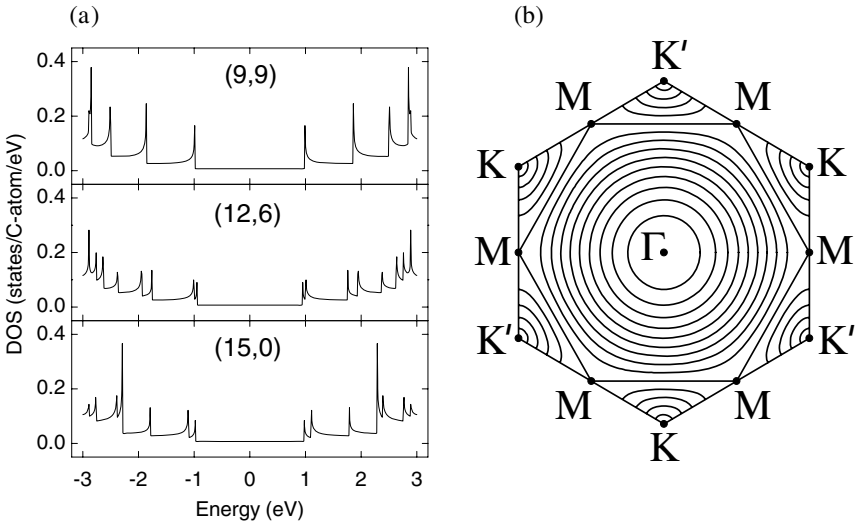

Figure 2. (a) The 1D electronic density of states for the valence and conduction bands versus energy (the Fermi level is at $E = 0$) for three metallic nanotubes of approximately the same diameter, showing the effect of chirality and trigonal warping (see the text) on the energies where the VHS occur in the density of states: (9, 9) (armchair), (12, 6) (chiral), and (15, 0) (zigzag). The plots are made using the tight binding approximation, assuming that the energy overlap integral is $\gamma_0 = 2.9$ eV and the wavefunction overlap integral vanishes, i.e. $s = 0$ [6]. (b) Plot of the 2D equi-energy contours in the 2D Brillouin zone of graphite, showing trigonal warping effects in the contours, as we move from the K point in the K–Γ or K–M directions. The equi-energy contours are circles near the K point and near the centre of the Brillouin zone Γ, but near the M points on the zone boundary the contours are straight lines which connect the nearest M points [8].

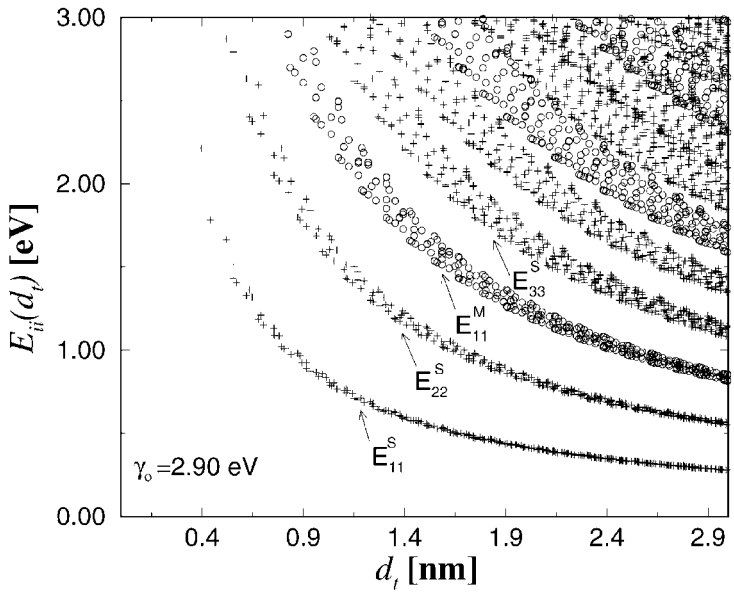

Figure 3. Calculated [8, 9] energy separations E_{ii} between VHS i in the 1D electronic density of states of the conduction and valence bands for all possible (n, m) values versus nanotube diameter in the range 0.4 nm $< d_t <$ 3.0 nm, using a value for the carbon–carbon energy overlap integral of $\gamma_0 = 2.9$ eV and a nearest-neighbour carbon–carbon distance $a_{C–C} = 1.44$ Å for making this plot [10, 8]. Semiconducting (S) and metallic (M) nanotubes are indicated by crosses and open circles, respectively. The subscript $i = 1$ denotes the index of the lowest energy of a singularity in the JDOS.

the information needed for the complete (n, m) assignment for a given SWNT. By combining information about E_{ii} with the diameter dependence of the vibrational mode, it is possible to correlate the Raman spectral properties with the electronic structure of those particular nanotubes that are resonantly excited by the laser, thereby providing a sensitive tool for probing the electronic structure and modifications to this structure by defects or surface functionalization.

3. Raman spectra for carbon nanotubes

3.1. Generalities

Early Raman spectroscopy studies on carbon nanotubes were performed on bulk samples containing nanotubes in the form of ropes or bundles and led to the use of the diameter selective resonance process to provide information about

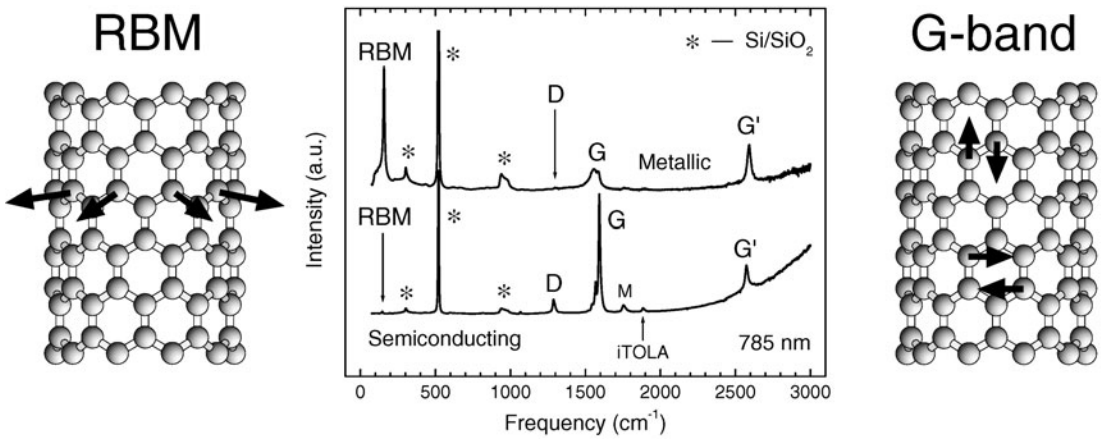

Figure 4. Raman spectra from a metallic (top) and a semiconducting (bottom) SWNT at the single nanotube level using 785 nm (1.58 eV) laser excitation, showing the RBM, D-band, G-band and G′-band features, in addition to weak double-resonance features associated with the M band and the iTOLA second-order modes [20]. Insets on the left and the right show atomic displacements associated with the RBM and G-band normal mode vibrations. The isolated carbon nanotubes are sitting on an oxidized silicon substrate which provides contributions to the Raman spectra denoted by '*' which are used for calibration purposes.

the diameter distribution of nanotubes in a SWNT bundle [11]. Raman spectroscopy is also of historical importance to nanotube research because at an early date the distinctive differences in the spectral lineshapes observed for SWNT bundles provided clear experimental proof of the predicted electronic structure [12] and allowed metallic and semiconducting SWNTs to be distinguished by their distinctly different lineshapes [13]. Concurrently, joint scanning tunnelling microscopy (STM) and scanning tunnelling spectroscopy (STS) [14, 15] studies corroborated the main conclusions of the Raman results, and each technique provided important complementary information.

Besides the success of using Raman spectroscopy for characterizing the diameter distribution and the metallic/semiconducting nanotube content within SWNT bundles [4, 13], a new research field in SWNTs was opened up by the observation of Raman spectra from just one nanotube, made possible by the strong intensity enhancement effect that occurs when the energy of the incident or scattered photon is in resonance with an interband transition from the valence band state i to a conduction band state i for light polarized along the nanotube axis ($\hat{z}$). The resonance enhancement of the Raman signal for a 1D system is very large [16] because each nearly discrete level (van Hove singularity) contains a large number of electrons that can absorb light at the resonant frequency and it is thus possible to see Raman spectra from just one isolated single-wall carbon nanotube [17]. Figure 4 shows typical Raman spectra from one isolated semiconducting (lower trace) and one isolated metallic (upper trace) single-wall carbon nanotube on a Si/SiO_2 substrate.

The four most important features seen in figure 4 are the radial breathing mode (RBM), whose frequency ω_{RBM} is related to the nanotube diameter by $\omega_{\mathrm{RBM}} \propto 1/d_{\mathrm{t}}$ and for which the carbon atoms are all vibrating in phase in the radial direction of the nanotube (see left inset to figure 4 to view the atomic displacements associated with the RBM), the tangential G band which is derived from the in-plane Raman-active mode in graphite (see right inset to figure 4 to view the atomic displacements associated with the G band), the disorder-induced D band and its second-order harmonic, the G′ band. As can be seen in figure 4, the Raman signal from one nanotube, $\sim$1 nm in diameter, is of comparable intensity to the signal from the silicon substrate atoms, which are approximately 10^6 times more numerous within the laser spot size of ~ 1 μm in diameter. Most of the single-nanotube spectroscopy studies thus far have been carried out on isolated tubes sitting on a Si/SiO_2 substrate [5]. However, Raman experiments have been recently reported for SWNTs in solution. These special solubilized SWNTs were obtained by dispersing SWNT bundles with an ultracentrifuge, resulting in isolated SWNTs surrounded by a coating of the surfactant sodium dodecyl sulfate (SDS), thus forming micelles around each SWNT [18]. This use of a surfactant around the nanotube allows the observation of the luminescence spectra from nanotubes in solution.

The Raman spectra in figure 4 at the single-nanotube level provide important information for one interested in both basic and applied carbon nanotube science. As mentioned above, the resonance Raman effect provides a characterization tool for the nanotube structure (n, m) at the single-nanotube level. For an isolated SWNT sitting on a Si/SiO_2 substrate, the constant α in $\omega_{\mathrm{RBM}} = \alpha/d_{\mathrm{t}}$ has been determined to be 248 cm^{-1} nm [17]. Because of the diameter-selective resonance Raman effect [3], study of the RBM frequencies for various E_{laser} values can be used for characterizing the diameter distribution of SWNTs in a sample of SWNT bundles [19]. Inspection of the two spectra in figure 4 indicates a distinctly different G-band lineshape, which can be used to distinguish metallic from semiconducting nanotubes, at the single-nanotube level or in SWNT bundles [13].

Of great interest for one working with nanotube samples in the context of applications are the D-band spectral properties, because the D band carries important information about the crystalline quality of the samples. The disorder-induced D band is only activated in the Raman spectrum of sp^2 carbons in the presence of hetero-atoms, vacancies, grain boundaries or any defect that lowers the crystal symmetry of the quasi-infinite lattice, thus relaxing the $q \sim 0$ zone-centre selection rule for the first-order Raman scattering process. The D-band intensity and linewidth can be used as a handy probe for measuring the

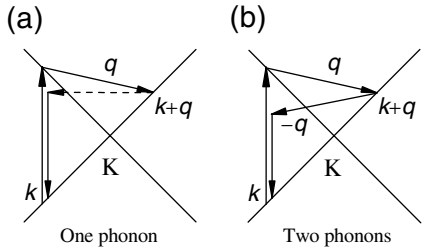

Figure 5. The *intravalley* double-resonance Stokes process near the K point in the 2D graphite Brillouin zone. (a) The scattering process for activating a defect-induced mode where the resonance is with the incident photon. The broken line indicates the elastic scattering by a defect. (b) The scattering process for the second-order modes. Other possible scattering events, not shown in the figure, involve elastic scattering first and phonon scattering second for the D-band, resonance with scattered photons, and anti-Stokes processes [21]. The D band and G′ band are both activated with similar processes, respectively, as in (a) and (b), but involve scattering from the K to K′ point (*intervalley* process).

degree of disorder in SWNTs. The physical origin of this mode is based on a double-resonance mechanism that couples electrons and phonons, and pertinent background on this topic is provided in the next section.

3.2. Double resonance in graphite

Before discussing the nanotube D-band properties explicitly, we first briefly introduce the double-resonance model for two-dimensional (2D) graphite, which is a zero bandgap semiconductor with a special electronic structure associated with its linear k-dependent energy bands near the hexagonal corner of the Brillouin zone (K point), where the valence and conduction bands cross and thus are degenerate. Optical processes in the visible range occur around the zone edge and the linear k electronic dispersion relations give rise to a very special resonance Raman effect. This effect, called the double-resonance effect in sp^2 carbon materials [22–25], is responsible for activating several phonon modes within the Brillouin zone that are not Raman-active in the first-order process. The dispersive D and G′ modes are the double-resonance modes that have been very intensively studied since the 1970s [26] in sp^2 carbons. The mechanisms responsible for the activation of the D and G′ modes are quite similar, the basic difference being that the D mode involves a phonon and a defect, while the G′ mode involves two phonons at wavevectors $\boldsymbol{q}$ and $-\boldsymbol{q}$. The intravalley resonance process analogous to the intervalley D process is depicted in figure 5(a), for the D-band process, and the corresponding analog to the G′-band process is indicated in figure 5(b). The electrons have initial wavevectors $\boldsymbol{k}$ (measured from the K point in the 2D graphite Brillouin zone) and also a scattered electronic state with wavevector $\boldsymbol{k}+\boldsymbol{q}$ (where $\boldsymbol{q}$ is the phonon wavevector), which satisfies the energy–momentum conservation relation

$$E(\boldsymbol{k}+\boldsymbol{q}) = E(\boldsymbol{k}) \pm \hbar\omega_{\mathrm{ph}}(\boldsymbol{q}). \tag{1}$$

Here $\pm$ corresponds to the Stokes ($-$) and anti-Stokes ($+$) processes. Energy and momentum conservation requirements select two possible equi-energies $E(\boldsymbol{k}+\boldsymbol{q})$, where the electrons have $\boldsymbol{k}+\boldsymbol{q}$ wavevectors. One of these equi-energies $E(\boldsymbol{k}+\boldsymbol{q})$ exists around the same K point as the initial state $\boldsymbol{k}$ (intravalley process) and the second $E(\boldsymbol{k}'+\boldsymbol{q})$ is located around the inequivalent K′ (intervalley process) point in the first Brillouin zone for 2D graphite. After absorption of the incident photon and scattering by phonons, electrons in the state $\boldsymbol{k}+\boldsymbol{q}$ are elastically scattered by an impurity or defect to a final state with the wavevector $\boldsymbol{k}$. After this, the electron–hole pair recombination occurs and the scattered photon is created. The scattering by the phonon and impurity/defect can occur in either order. For the G′ band, which involves two phonons with $\boldsymbol{q}$ and $-\boldsymbol{q}$ wavevectors, electrons in the $\boldsymbol{k}+\boldsymbol{q}$ states are now inelastically scattered to a final state with wavevector $\boldsymbol{k}$. Of particular importance, the energy and momentum conservation requirements lead to a relation between the $\boldsymbol{k}$ for electrons and the $\boldsymbol{q}$ for phonons. By searching for a double-resonance process that satisfies the condition in equation (1) within the Brillouin zone of graphite, and by neglecting the trigonal warping effect [24] for simplicity, it is found that $\boldsymbol{q}$ values that strongly contribute to the double-resonance condition are preferentially located near $|\boldsymbol{q}-\boldsymbol{q_0}| \sim 2k$ [27] where $\boldsymbol{q_0}$ is the phonon wavevector between the K and K′ points in the 2D Brillouin zone. This relation is special and causes different incident photon energies (E_{laser}) to excite different $\boldsymbol{k}$ states, which in turn change the magnitude of the phonon wavevector, thus allowing one to use phonons to probe both the energy and the wavevector in the electronic dispersion relations through the strong electron–phonon coupling, that occurs under resonance Raman conditions. This simple relation between the electronic wavevector $\boldsymbol{k}$ and phonon wavevector $\boldsymbol{q}$ has some restrictions in the case of carbon nanotubes, because of the quantum confinement effect that restricts the number of available states, and this is discussed in the next section.

3.3. Dispersive modes in carbon nanotubes

The dispersive disorder-induced D mode in SWNTs is also very important for characterizing SWNTs, because its properties, including its frequency, intensity and linewidth, carry information about SWNT electronic properties, their compressive or tensile strain and the degree of structural disorder of the SWNT. Such information turns out to be decisive for achieving high mechanical performance in nanotube-based composites, thereby allowing use of this mode for characterizing, and also monitoring, the purification process of SWNTs. The observation of the second-order G′ band (a D-band overtone) is not defect-dependent, but its frequency, intensity and linewidth are strongly dependent on compressive and tensile strain, with observed pressure coefficients for the G′-band frequency in SWNT bundles of 23 cm^{-1} GPa^{-1} (under compression) and -13 cm^{-1} GPa^{-1} (under tension) [28–30]. These properties can be used to characterize nanotubes, making Raman spectroscopy a sensitive technique for verifying the presence of either compressive or tensile strain effects for SWNTs dispersed in composites.

It should be pointed out that it is not only the D band that carries information about disorder, impurities and defects in the sp^2 carbon material, but also several other low intensity Raman modes carry such information, and these modes have been recently identified as double-resonance modes induced by defects [24].

In the case of multiwall carbon nanotubes, a mode observed at about 1620 cm^{-1} (and called the D* band) also carries information about disorder in the sp^2 lattice and this mode is also observed in graphite [31]. Double-resonance theory is also able to assign this feature, as shown by Tan *et al* [32], as a contribution from different phonon wavevectors near the maximum frequency of the graphite phonon dispersion relations near the Γ point rather than near the K point, as occurs for the D band. The analysis of Tan *et al* [32] shows that the D* feature depends on the number of defects in the carbon nanotube sidewall. This comes from the fact that, to activate the mode that involves only one phonon scattering event via the double-resonance effect, the process outlined in figure 5(a) requires the scattering of the electron by a defect, and the intensity of this process is proportional to the number of defects present in the sample, thus giving rise to a more intense D*-band feature in the Raman spectra as the disorder increases. Some second-order combination and overtones modes are also activated due to double-resonance effects [20]. However, we focus our discussion here on the D-band properties for getting information about nanotube defects because the D-band is the strongest of the defect-induced modes.

4. Application of Raman spectroscopy

There is currently interest in the application of single-walled carbon nanotubes for reinforcement in fibre and polymer composites whereby nanotubes act as strengthening building blocks. The way this issue has been addressed technologically is just by mixing single-walled carbon nanotubes with different polymer matrices and the nanotube–polymer cohesion comes from the van der Waals interaction. By creating such covalent bonds, nanotubes are expected to improve the mechanical properties of the composites, and either the defects or chemical species attached to the nanotube surface should play a fundamental role in designing the desired and optimal properties of such composite materials and in controlling the degree of strengthening by the nanotubes through controlling either the density of nanotube defects or the density of chemical species attached to the nanotube. Another variable that could contribute to the materials design would be the diameter of the tube through its chemically active surface that should be closely related to nanotube curvature effects, as is also observed for fullerenes [33].

In this scenario it is highly desirable to gain an understanding of the mechanisms responsible for the properties of the D-band Raman feature in both semiconducting and metallic tubes and the dependence of these properties on the nanotube structure. This very fundamental understanding in turn can be used to better characterize these nanotube–polymer based composites. Some properties of the D band in SWNT bundles have been probed by using single-nanotube spectroscopy, as we discuss in the next subsection.

4.1. D-band diameter dependence in single-wall nanotubes

Figure 6(a) shows data (for both semiconducting (S) and metallic (M) tubes probed with $E_{\rm laser} = 2.41$ eV) for the D-band frequency $\omega_{\rm D}$ for isolated SWNTs plotted versus $1/d_{\rm t}$ for different interband electronic transitions E_{ii}, between the

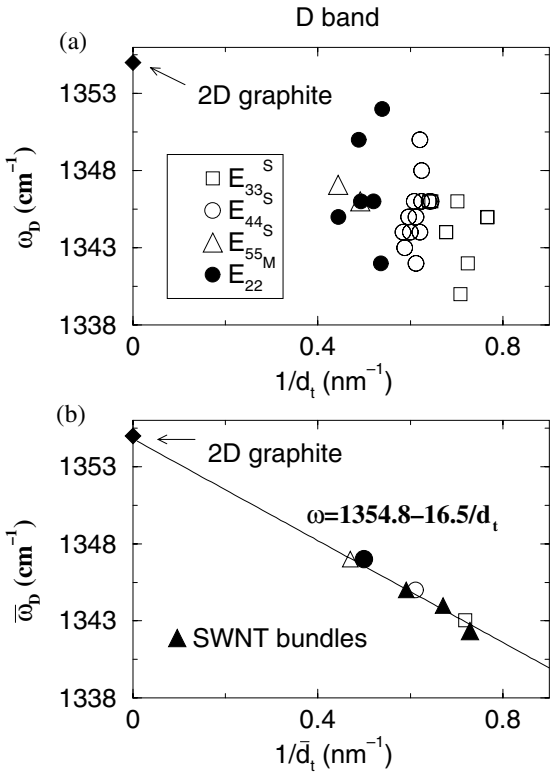

Figure 6. (a) D-band frequencies as a function of reciprocal diameter for individual SWNTs using $E_{\rm laser} = 2.41$ eV laser excitation. The data are classified in terms of the E_{ii} interband transition with which the resonance occurs, including both metallic (M) and semiconducting (S) SWNTs. (b) Plot of $[\bar{\omega}_{\rm D}(E_{ii})]$, denoting the observed D-band frequencies averaged over all tubes resonant with a given interband transition E_{ii}, versus $1/\bar{d}_{\rm t}$, denoting the corresponding average of the reciprocal diameter of the tubes. Data are shown for $E_{\rm laser}$ in resonance with the $E_{55}^{\rm S}$, $E_{44}^{\rm S}$, $E_{33}^{\rm S}$ and $E_{22}^{\rm M}$ electronic interband transitions. The line is a fit to the data, showing that the D-band frequencies extrapolate (on average) to the graphene (2D graphite) value when $1/\bar{d}_{\rm t} \to 0$. The full triangles in (b) denote the D-band frequencies for three different SWNT bundles with different average diameters [37–39].

singularities in the joint density of states (JDOS)[8]. Although these data are all taken with the same laser excitation energy, the data points do not show a definitive pattern. We can, however, see that $\omega_{\rm D}$ for isolated SWNTs has lower values than $\omega_{\rm D}$ for 2D graphite (1355 cm^{-1} taken from [34], as shown by the full diamond-shaped point in figure 6). The data points in figure 6(a) seem to extrapolate roughly to the 2D graphite value when $d_{\rm t} \to \infty$, i.e. $(1/d_{\rm t}) \to 0$ [34, 35]. However, the experimental measurements for the dependence of $\omega_{\rm D}$ on the diameter $d_{\rm t}$ (see figure 6(a)) do not deliver a clear message when taken by themselves at the single-nanotube level but, as is shown below, these data are very useful for understanding the corresponding effect in SWNT bundles. In particular, the spread in the data points in figure 6(a) is associated with the chirality dependence [36] of the k_{ii} states as a consequence of both the trigonal warping effect [8] (anisotropy in the electronic band structure) and the double-resonance process [22, 24].

[8] The joint density of electronic states (JDOS) is given by $\mathrm{JDOS}(\hbar\omega) = (1/4\pi^3)\int \delta[E_i^{\rm c}(k) - E_i^{\rm v}(k) - \hbar\omega]\,{\rm d}k$, where $E_i^{\rm c}$ and $E_i^{\rm v}$ are the energies for the ith electronic state in the conduction (c) and valence (v) bands, respectively.

What we mean by the chirality dependence of ω_D for SWNTs is that different nanotubes with different θ values will be resonant at the same E_{laser} value, thus giving rise to a range of ω_D values, whereas for sp^2 carbons and graphite, there is a single ω_D for a given E_{laser}. A similar behaviour is observed for the $1/d_t$ dependence of $\omega_{G'}$. In [36] a clear dependence of ω_D on chiral angle θ was reported for nanotubes with a similar diameter, whereas ω_{RBM} and ω_G do not show any significant dependence on θ [5].

In order to correlate the results for $\omega_D(d_t)$ at the single-nanotube level with those for SWNT bundles and to gain an understanding of the mechanisms behind the d_t dependence of the D-band frequency, we average over the chirality-dependent ω_D data for the isolated SWNTs shown in figure 6(a) for a given interband transition E_{ii}, over which the d_t values show only a small variation. We denote the resulting averages of the diameter and D-band frequencies by $\bar{d}_t(E_{ii})$ and $\bar{\omega}_D(E_{ii})$, respectively, and we plot these pairs of numbers in figure 6(b) for $i = 3, 4, 5$ for semiconducting and for $i = 2$ for metallic SWNTs, using the same symbols as in figure 6(a).

The results of this analysis in figure 6 give a simple linear dependence of the average $\bar{\omega}_D$ on $1/\bar{d}_t$, i.e.

$$\bar{\omega}_D = 1354.8 - 16.5/\bar{d}_t, \tag{2}$$

where $1/\bar{d}_t$ is the average of $1/d_t$, as shown in figure 6(b). We also obtain very good agreement in figure 6(b) between the $\bar{\omega}_D$ results for isolated tubes and the corresponding $\bar{\omega}_D$ results for SWNT bundles measured with the same E_{laser}. The full triangles in figure 6(b) denote the average $\bar{\omega}_D$ for SWNT bundles with different average SWNT reciprocal diameters $1/\bar{d}_t$, as given in [37–39]. The results of figure 6(b) show that $\bar{\omega}_D(E_{ii})$ for isolated SWNTs and $\bar{\omega}_D$ for SWNT bundles both increase when d_t increases, and both data sets yield the same functional form. The linear downshift of $\bar{\omega}_D$ as a function of $1/\bar{d}_t$, shown in figure 6(b), is attributed to the softening of the spring constants for the vibrations associated with the D band due to the nanotube curvature, and the complicated dependence at the single-nanotube level (spread in figure 6(a)) comes from the different electronic states associated with each VHS (each SWNT with its own wavevector k_{ii}), due to the trigonal warping effect [8].

Another remarkable result shown in figure 6 concerns the D-band diameter dependence for metallic and semiconducting tubes. The results suggest that metallic and semiconducting tubes have the same spring constant dependence on nanotube curvature and that they therefore follow the same ω_D diameter-dependent behaviour.

For practical purposes it is interesting to get information about the nanotubes and their environmental conditions by looking at the D-band second-order related feature, the G′ band. The presence of this mode does not depend on defects and it is very intense and easily observable in the Raman spectra. Furthermore, the G′ band exhibits a large dispersion either when the laser energy is changed or when compressive and tensile strains are applied. Due to this sensitivity, a small perturbation to either the electronic structure or the environment around a nanotube will be detected in the G′-band spectra through changes in its lineshape, frequency and intensity. By now applying the same approach that was previously applied to the D band to the second-order G′ band, which appears at a frequency of approximately $2\omega_D$, a fit to the experimental results (measured with $E_{laser} = 2.41$ eV) leads to

$$\bar{\omega}_{G'} = 2708.1 - 35.4/\bar{d}_t, \tag{3}$$

in analogy to the D-band results for SWNTs (equation (2)). Both the frequency intercept at $1/\bar{d}_t \rightarrow 0$ and the slope for the G′-band data is consistent with the corresponding D-band behaviour, based on the approximate relation $\omega_{G'} \simeq 2\omega_D$. Furthermore, the G′-band frequency of 2D graphite is 2710 cm^{-1} (taken from [34]), which is close to 2708.1 cm^{-1}, and the slope of 35.4 cm^{-1} nm in equation (3) is close to twice the D-band slope of 16.5 cm^{-1} nm in equation (2).

It should be mentioned here that other groups have proposed a theory that does not consider the resonant factor coming from the VHS, but they rather consider only the double-resonance process to be responsible for the D-band and G′-band features and they state that the process is allowed only in metallic-2 type tubes [40]. Metallic-1 tubes occur when $n - m$ is not a multiple of $3d$ and metallic-2 if $n - m$ is a multiple of $3d$, where d is the largest common divisor of n and m [6]. This prediction is not consistent with a huge amount of experimental results on isolated SWNTs, whereby the G′ band is clearly observed in all kind of nanotubes [5], i.e. semiconducting, metallic-1 and metallic-2. A theory considering the double-resonance process and including resonance with VHS was reported by Kürti *et al* [25] and this theory predicts that all tubes can exhibit a D band, thereby also explaining the anomalous dispersion observed in SWNT bundles. Effort is now being expended to bring convergence between these different interpretations.

4.2. Functionalizing carbon nanotubes

In addition to their exotic physical properties, sp^m ($2 < m < 3$) hybridized carbons have been found to exhibit interesting chemical properties [31, 41]. For instance, fullerene chemistry blossomed into a rich sub-field of its own, allowing researchers to develop recipes for fullerene purification, chromatographic separation and functionalization in order to yield fullerenes with tailored chemical properties [33, 41, 42]. Since carbon nanotubes are closely related to fullerene molecules, it is natural to expect that the chemical functionalization of carbon nanotubes would also become an important research area [43], stimulated by the strong gas adsorption properties of SWNTs, either on their external surfaces [44, 45] or possibly within their nano-capillaries [46, 47]. However, some barriers had to be overcome before the functionalization of SWNTs could become a reality, because of the insolubility of as-prepared carbon nanotubes in water or in organic solvents. This chemical inertness is due to the strong covalent bonds of the carbon atoms to each other on the nanotube surface. Nevertheless, much progress has been made recently in the chemical functionalization of SWNTs for various applications [43, 48].

We now discuss how the opening of the C–C covalent bonds by functionalization changes both the frequencies and intensities of the Raman features of carbon nanotubes. It is expected that the chemical attachment of chemical species (whether it is an inorganic species, such as an alkali metal donor, or a halogen acceptor, a polymer chain or a DNA strand) to the sidewall of a nanotube will perturb its Fermi

level through charge transfer effects. Since electrons and phonons are strongly coupled to each other in resonance Raman spectroscopy, it is expected that such perturbations should be visible in the various Raman modes of the carbon nanotubes as a result of charge transfer effects associated with chemical species, similar to what occurs generally in sp^2 carbons through the graphite intercalation process [31]. In section 4.3, we consider the effect on the Raman spectra of doping SWNT bundles with donors and acceptors. In section 4.4, we discuss the effect of an external applied potential in an electrochemical cell. These basic studies on the use of Raman spectroscopy to characterize the functionalization of nanotubes have been carried out thus far primarily on SWNT bundles. It is expected that similar studies at the single-nanotube level will soon be available to provide more detailed information on the role of nanotube diameter and chirality in the functionalization process and on differences in behaviour between metallic and semiconducting tubes.

4.3. n- and p-doping effects

One method for assessing how chemical species perturb the nanotube electronic properties is by carrying out donor or acceptor doping experiments where either electrons or holes are added to the nanotubes. For the case of SWNT bundles doped with halogen acceptors (for example, Br_2), frequency upshifts are observed for both ω_{RBM} and ω_{G^+}, respectively, by $\sim$74 and $\sim$24 cm^{-1}, relative to the corresponding frequencies in the undoped SWNT bundles [49, 50]. On the other hand, doping with alkali metals, like K or Rb, leads to a softening (or downshift) of ω_{RBM} and ω_{G}, accompanied by dramatic changes in the lineshape for the tangential G band. For example, the G-band frequency in saturation K-doped or Rb-doped bundles becomes very broad, downshifts by $\sim$35 cm^{-1} and exhibits a characteristic Breit–Wigner–Fano lineshape [49]. Furthermore, the RBM band in saturation K-doped or Rb-doped bundles is not evident in the Raman spectrum. The RBM band in such alkali metal-doped SWNTs may have shifted to very low frequencies or it may have broadened to such an extent that it could not be distinguished from the noise. These shifts provide evidence for charge transfer between the dopants and SWNT bundles, indicating an ionic character for the dopant–SWNT bonds. Doping with halogens transfers electrons from the π states in the SWNTs to the halogens, creating hole carriers in the SWNTs and making the SWNTs p-type. Likewise, alkali metal dopants transfer electrons to the π^* states, making the nanotubes n-type. From a theoretical standpoint, these results have been explained within the framework of a rigid band model, whereby it is assumed that there is no modification to the E_{ii} values of a SWNT through the doping process, but the Fermi level is shifted very significantly by the addition of electrons and holes [11, 51, 52].

These Fermi level tuning experiments have provided fundamental information about the available states necessary for satisfying the Pauli principle for the resonance Raman process [7]. The intensity of the Raman features drastically decreases when the initial state gets depleted of carriers and the final state is filled with carriers [53]. A more detailed assessment to what is happening in the SWNT–chemical species interaction might be achieved by carrying out experiments at the functionalized single-nanotube level. By correlating these studies with the knowledge developed so far for undoped SWNTs at the single-nanotube level, it should be possible to get fundamental information regarding the charge transfer process and the types of defects that are introduced in such doping experiments by analysing the changes in the frequency, intensity and linewidth that different chemical species introduce into the various Raman features, and the dependence of the Raman spectra on nanotube diameter and chirality.

4.4. External bias effects

Studies of the electrochemical potential combined with optical experiments (optical absorption, infrared and Raman spectroscopy) in carbon nanotubes have been performed in bulk samples containing SWNT bundles [55–58]. From these studies it was proposed that the anodic (cathodic) potential depletes (fills) the valence (conduction) band states of the SWNTs. Since resonant Raman spectroscopy strongly depends on the transition from valence states to conduction states, the effect of the depletion/filling of electronic states turns out to be very effective in changing the Raman spectra properties, so that these electrochemical experiments provide a method for continuously tuning the Fermi level. Figure 7(a) shows the change in the spectra at $E_{\mathrm{laser}} = 1.96$ eV for SWNT bundles ($d_{\mathrm{t}} = 1.25 \pm 0.20$ nm) cast on a Pt electrode substrate immersed in an H_2SO_4(0.5 M) aqueous solution as the external voltage V is varied from 0 to +1.3 V and then back to 0 V. While the dependences of ω_{D}, ω_{G} and $\omega_{\mathrm{G}'}$ on V were all studied, it was found that the dependence of $\omega_{\mathrm{G}'}$ on V presented the clearest characterization probe for the charge transfer process. The experimental results for $\omega_{\mathrm{G}'}$ versus V could be explained quantitatively in terms of the lowering of the Fermi level with increasing V, thereby emptying states from VHS in the valence band and, in the case of metallic tubes, also from the constant non-zero density of states between the lowest energy pair of VHS E_{11}^{M}, as shown in figure 7(b). The good agreement between experiment and theory regarding the dependence of $\omega_{\mathrm{G}'}$ on V and the observation of a different behaviour for semiconducting and metallic tubes indicates that the applied voltage V has only a small effect on the energy of the VHS, but that the application of V mainly affects the occupation of valence and conduction band states [54]. It is thus shown that the external potential strongly affects the filling of electron or hole states, resulting in large shifts of the various mode frequencies and in the suppression of interband transitions as initial states are emptied or final states are filled [58]. The effect of positive and negative applied potentials is similar to that of chemical doping discussed in section 4.3, insofar as the values of E_{ii} do not change much, but large shifts in Fermi level (the filling and emptying of electron states) are observed.

It should be pointed out that the dramatic changes observed in the Raman spectra in figure 7 occur only for cases where the electrolyte intercalates between the bundles. When this is not the case, the changes in the Raman spectra may be very small, indicating that the electrochemical reaction occurs at the external surface of the SWNT bundle.

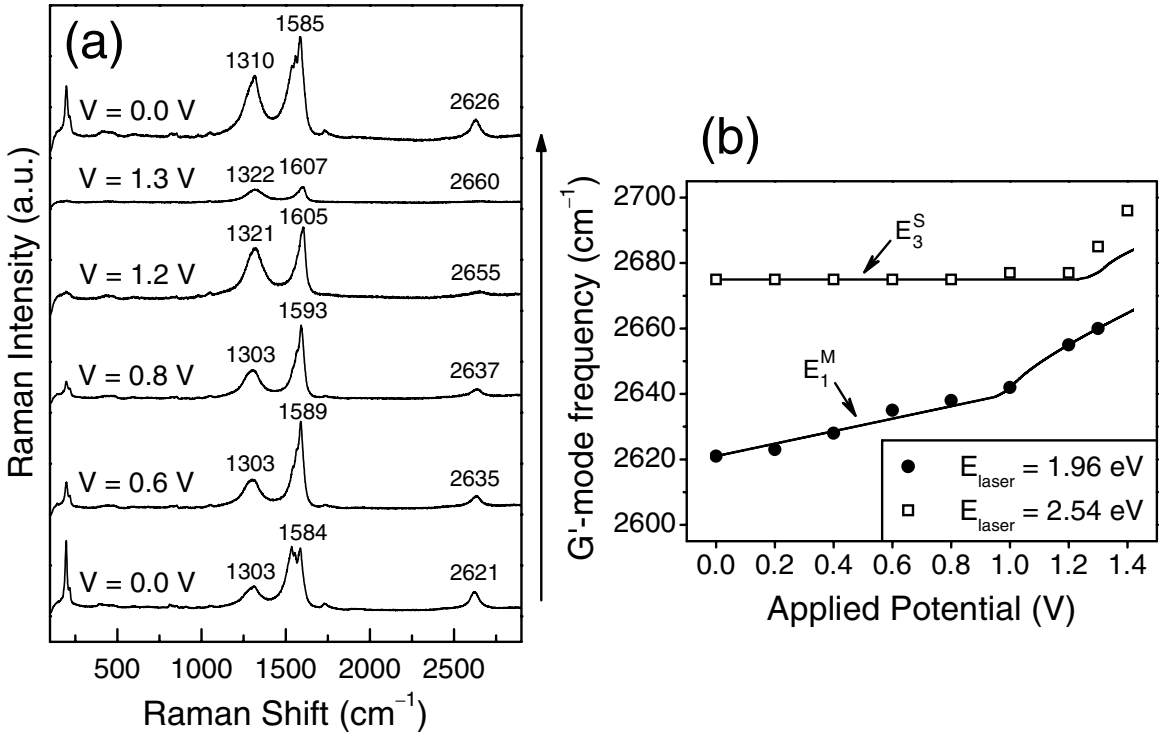

Figure 7. (a) *In situ* Raman spectra of a SWNT film cast on a platinum electrode surface in an H_2SO_4 0.5 M aqueous solution. The spectra are obtained at the indicated positive applied potentials and $E_{laser} = 1.96$ eV. The frequencies for the dominant G-band, D-band and G′-band features are indicated in cm^{-1}. (b) The points denote G′-band frequencies for the same SWNT film as in (a), obtained at the indicated applied potentials for $E_{laser} = 1.96$ and 2.54 eV. The full curves in (b) are theoretical curves for the G′-band mode frequency calculated from charge transfer based on the SWNT density of states as the Fermi level (electrochemical potential) varies with applied voltage (reprinted from [54]).

5. Concluding remarks

In this paper we have discussed how resonance Raman spectroscopy in single-wall carbon nanotubes can be used to sensitively probe the various modifications that can be introduced on the nanotube surface, such as defects due to purification processes and charge transfer effects from chemical species attached to the side wall. Both types of modifications are fundamental for thinking about nanotube applications, because the introduction of defects can break covalent bonds which introduce chemical reactivity to the nanotube. On the other hand, the functionalization process itself requires defects for attaching foreign species to the nanotube side wall and the choice of the optimal chemical species for coupling nanotubes to other systems is a key for integrating nanotube technology with other currently available technologies. The sensitivity of the Raman spectra along with its advantages (as a non-invasive, contactless, readily available probe) to characterize nanotubes in all kinds of environments to which nanotubes might be exposed, makes Raman scattering a useful tool for characterizing nanotubes used in devices. Such use will in turn provide feedback for the improvement and development of new materials systems through aiding with the design of desired properties. Resonance Raman spectroscopy thus provides a sensitive tool for probing and characterizing the defects associated with functionalization by analysing the detailed characteristics of the disorder-induced modes, mainly the D band, that is the most intense, while charge transfer effects should be detected through changes in the frequencies of the various modes, such as the G band and G′ band.

Electrochemistry studies at the single-nanotube level are expected to answer open issues about the nanotube–electrode interface interaction because, in contrast to the SWNT bundle samples, the Fermi level alignment of the isolated nanotube–electrode junction will not have contributions from the capacitive charging effects observed for SWNT bundle samples. Raman studies at the single-nanotube level will also allow separate study of the effects of the external potential on metallic and semiconducting tubes through detailed monitoring of the various features in the resonance Raman spectra (intensities, lineshapes and frequencies).

The increasing development of near-field optical technology and the association of this technique with Raman spectroscopy will allow detailed study of the SWNT surface both with high spatial and spectral resolution [59, 60]. This will provide the opportunity for identifying, analysing and acquiring spatially-resolved defect and chemical maps of the nanotube surface. This topographical localization of the scattering centres, combined with the knowledge developed so far for Raman scattering in nanotubes, is expected to provide a deeper understanding of the nanotube surface and its related chemistry in the near future.

Acknowledgments

The authors acknowledge Professsors A M Rao, P Corio, M A Pimenta, A K Swan, J Mendes Filho and Ms Shin G Chou

for valuable discussions on the many topics of Raman scattering in carbon nanotubes. AGSF and AJ acknowledge financial support from the Brazilian agencies CAPES (PRODOC grant 22001018) and CNPq, respectively. The MIT authors acknowledge support under NSF grants DMR 01-16042 and INT 00-00408. RS acknowledges a Grant-in-Aid (no 13440091) from the Ministry of Education, Japan.

References

[1] Dresselhaus M S, Dresselhaus G, Pimenta M A and Eklund P C 1999 *Analytical Applications of Raman Spectroscopy* (Oxford: Blackwell) p 367
[2] Ferrari A C 2002 *Diamond Relat. Mater.* **11** 1053
[3] Rao A M, Richter E, Bandow S, Chase B, Eklund P C, Williams K W, Fang S, Subbaswamy K R, Menon M, Thess A, Smalley R E, Dresselhaus G and Dresselhaus M S 1997 *Science* **275** 187
[4] Dresselhaus M S and Eklund P C 2000 *Adv. Phys.* **49** 705
[5] Dresselhaus M S, Dresselhaus G, Jorio A, Souza Filho A G and Saito R 2002 *Carbon* **40** 2043
[6] Saito R, Dresselhaus G and Dresselhaus M S 1998 *Physical Properties of Carbon Nanotubes* (London: Imperial College Press)
[7] Saito R and Kataura H 2001 *Top. Appl. Phys.* **80** 213
[8] Saito R, Dresselhaus G and Dresselhaus M S 2000 *Phys. Rev.* B **61** 2981
[9] Kataura H, Kumazawa Y, Maniwa Y, Umezu I, Suzuki S, Ohtsuka Y and Achiba Y 1999 *Synth. Met.* **103** 2555
[10] Dresselhaus G, Pimenta M A, Saito R, Charlier J C, Brown S D M, Corio P, Marucci P and Dresselhaus M S 2000 *Science and Applications of Nanotubes* (New York: Kluwer) p 275
[11] Rao A M, Eklund P C, Bandow S, Thess A and Smalley R E 1997 *Nature* **388** 257
[12] Saito R, Fujita M, Dresselhaus G and Dresselhaus M S 1992 *Appl. Phys. Lett.* **60** 2204
[13] Pimenta M A, Marucci A, Empedocles S, Bawendi M G, Hanlon E B, Rao A M, Eklund P C, Smalley R E, Dresselhaus G and Dresselhaus M S 1998 *Phys. Rev.* B **58** 16016
[14] Odom T W, Huang J L, Kim P and Lieber C M 1998 *Nature* **391** 62
[15] Wildöer J G W, Venema L C, Rinzler A G, Smalley R E and Dekker C 1998 *Nature* **391** 59
[16] Martin R M and Falicov L M 1983 *Top. Appl. Phys.* **8** 70
[17] Jorio A, Saito R, Hafner J H, Lieber C M, Hunter M, McClure T, Dresselhaus G and Dresselhaus M S 2001 *Phys. Rev. Lett.* **86** 1118
[18] Bachilo S M, Strano M S, Kittrell C, Hauge R H, Smalley R E and Weisman R B 2002 *Science* **298** 2361
[19] Kuzmany H, Plank H, Hulman M, Kramberger Ch, Grüneis A, Pichler Th, Peterlik H, Kataura H and Achiba Y 2001 *Eur. Phys. J.* B **22** 307
[20] Brar V W, Samsonidze Ge G, Dresselhaus G, Dresselhaus M S, Saito R, Swan A K, Ünlü M S, Goldberg B B, Souza Filho A G and Jorio A 2002 *Phys. Rev.* B **66** 155418
[21] Cançado L G, Pimenta M A, Saito R, Jorio A, Ladeira L O, Grüneis A, Souza Filho A G, Dresselhaus G and Dresselhaus M S 2002 *Phys. Rev.* B **66** 035415
[22] Thomsen C and Reich S 2000 *Phys. Rev. Lett.* **85** 5214
[23] Ferrari A C and Robertson J 2001 *Phys. Rev.* B **64** 075414
[24] Saito R, Jorio A, Souza Filho A G, Dresselhaus G, Dresselhaus M S and Pimenta M A 2002 *Phys. Rev. Lett.* **88** 027401
[25] Kürti J, Zólyomi V, Grüneis A and Kuzmany H 2002 *Phys. Rev.* B **65** 165433
[26] Tuinstra F and Koenig J L 1970 *J. Phys. Chem.* **53** 1126
[27] Saito R, Jorio A, Souza Filho A G, Dresselhaus G, Dresselhaus M S, Grüneis A, Cançado L G and Pimenta M A 2002 *Japan. J. Appl. Phys.* 1 **41** 4878
[28] Cooper C A and Young R J 1999 *J. Raman Spectrosc.* **30** 929
[29] Ajayan P M, Schadler L S, Giannaris C and Rubio A 2000 *Adv. Mater.* **12** 750
[30] Cooper C A, Young R J and Halsall M 2001 *Composites* A **32** 401
[31] Dresselhaus M S and Dresselhaus G 1981 *Adv. Phys.* **30** 139
Dresselhaus M S and Dresselhaus G 2002 *Adv. Phys.* **50** 1
[32] Tan P H, An L, Liu L Q, Guo Z X, Czerw R, Carroll D L, Ajayan P M, Zhang N and Guo H L 2002 *Phys. Rev.* B **66** 245410
[33] Hirsch A 1999 *Top. Curr. Chem.* **199** 1
[34] Wilhelm H, Lelausian M, McRae E and Humbert B 1998 *J. Appl. Phys.* **84** 6552
[35] Pimenta M A, Jorio A, Brown S D M, Souza Filho A G, Dresselhaus G, Hafner J H, Lieber C M, Saito R and Dresselhaus M S 2001 *Phys. Rev.* B **64** 041401
[36] Souza Filho A G, Jorio A, Dresselhaus G, Dresselhaus M S, Saito R, Swan A K, Ünlü M S, Goldberg B B, Hafner J H, Lieber C M and Pimenta M A 2002 *Phys. Rev.* B **65** 035404
[37] Pimenta M A, Hanlon E B, Marucci A, Corio P, Brown S D M, Empedocles S A, Bawendi M G, Dresselhaus G and Dresselhaus M S 2000 *Braz. J. Phys.* **30** 423
[38] Brown S D M, Jorio A, Dresselhaus M S and Dresselhaus G 2001 *Phys. Rev.* B **64** 073403
[39] Tan P H, Deng Y M, Zhao Q and Cheng W C 1999 *Appl. Phys. Lett.* **74** 1818
[40] Maultzsch J, Reich S and Thomsen C 2001 *Phys. Rev.* B **64** 121407
[41] Dresselhaus M S, Dresselhaus G and Eklund P C 1996 *Science of Fullerenes and Carbon Nanotubes* (New York: Academic)
[42] Geckeler K E and Samal S 1999 *Polym. Int.* **48** 743
[43] Niyogi S, Hamon M A, Hu H, Zhao B, Bhowmik P, Sen R and Itkis M E 2002 *Acc. Chem. Res.* **35** 1105
[44] Liu C, Fan Y Y, Liu M, Cong H T, Cheng H M and Dresselhaus M S 1999 *Science* **286** 1127
[45] Pradhan B K, Harutyunyan A R, Stojkovic D, Grossman J C, Zhang P, Cole M W, Crespi V, Goto H, Fujiwara J and Eklund P C 2002 *J. Mater. Res.* at press
[46] Hirsch A 2002 *Angew. Chem. Int. Edn Engl.* **41** 1853
[47] Eklund P C 2003 *Bulletin of the American Physical Society* vol 48 (New York: American Physical Society) p 589
[48] Sun Y P, Fu K, Lin Y and Huang W 2002 *Acc. Chem. Res.* **35** 1096
[49] Rao A M, Eklund P C, Bandow S, Thess A and Smalley R E 1997 *Nature* **388** 257
[50] Bandow S, Rao A M, Sumanasekera G U, Eklund P C, Kokai F, Takahashi K, Yudasaka M and Iijima S 2000 *Appl. Phys.* A **71** 561
[51] Dresselhaus M S, Rao A M and Dresselhaus G 2003 *Encyclopedia of Nanoscience and Nanotechnology* (Stevenson Ranch, CA: American Scientific Publishers) at press
[52] Rakitin A, Papadopoulos C and Xu J M 2003 *Phys. Rev.* B **67** 033411
[53] Jacquemin R, Kazaoui S, Yu D, Hassanien A, Minami N, Kataura H and Achiba Y 2000 *Synth. Met.* **115** 283
[54] Corio P, Santos P S, Brar V W, Samsonidze Ge G, Chou S G and Dresselhaus M S 2003 *Chem. Phys. Lett.* **370** 675
[55] Sumanasekera G U, Allen J L, Fang S, Loper A L, Rao A M and Eklund P C 1999 *J. Phys. Chem.* **103** 4292
[56] Kavan L, Raptar P and Dunsch L 2000 *Chem. Phys. Lett.* **328** 363
[57] An C P, Vardeny Z V, Iqbal Z, Spinks G, Baughman R H and Zakhidov A 2001 *Synth. Met.* **116** 411
[58] Minami N, Kazaoui S, Jacquemin R, Yamawaki H, Aoki K, Kataura H and Achiba Y 2001 *Synth. Met.* **116** 405
[59] Hartschuh A and Novotny L 2003 *Bulletin of the American Physical Society* vol 48 (New York: American Physical Society) p 388
[60] Hartschuh A, Sanchez E J, Xie X S and Novotny L 2003 *Phys. Rev. Lett.* **90** 95503